Low Excess Noise $Al_{0.8}In_{0.2}As_{0.31}Sb_{0.69}$ Avalanche Photodiodes Lattice Matched to InAs

G. Basta, T. Blain, J. Taylor-Mew, I.S. Han, M. Hopkinson, J.P.R. David, *Senior Member*, *IEEE*, J.S. Ng, *Member*, *IEEE*, C.H. Tan, *Senior Member*, *IEEE*

***Abstract*— Indium arsenide (InAs) is an exceptional material for absorbing infrared photons with wavelengths up to 3500 nm, making it ideal for mid-infrared detection. However, the development of high-performance Separate Absorption and Multiplication Avalanche Photodiodes (SAM APDs) has been hindered by the absence of suitable low-noise avalanche materials compatible with InAs absorbers. In this study, we investigate the potential of $Al_{0.8}In_{0.2}As_{0.31}Sb_{0.69}$ (lattice matched to InAs) as a low-noise avalanche material. We have performed comprehensive $Al_{0.8}In_{0.2}As_{0.31}Sb_{0.69}$ excess noise measurements using three optical signal wavelengths on a large number of p-i-n and n-i-p devices. Under pure electron injection, $Al_{0.8}In_{0.2}As_{0.31}Sb_{0.69}$ p-i-n diodes exhibit very low excess noise factors ~ 4 at high gain of 100, corresponding to an effective k of 0.02 - 0.03. In contrast, a small gain of 3 produces very high excess noise factors (> 17) when using hole injection in the n-i-p diodes. The contrasting behavior indicates that in $Al_{0.8}In_{0.2}As_{0.31}Sb_{0.69}$ electron ionization coefficient is much larger than hole ionization coefficient. As a consequence, low-noise $Al_{0.8}In_{0.2}As_{0.31}Sb_{0.69}$ avalanche regions emerge as a promising candidate for the avalanche region of SAM APDs designed for mid-infrared applications, such as methane gas sensing and imaging through fog. The design of such SAM APDs should ensure electrons rather than holes are injected into the $Al_{0.8}In_{0.2}As_{0.31}Sb_{0.69}$ avalanche regions to achieve the lowest possible excess noise factors.**

***Index Terms*—Avalanche photodiodes (APDs), AlInAsSb, infrared detectors, excess noise factor**

This work was supported by the U.K. Engineering and Physical Sciences Research Council under Grant EP/S026428/1. The review of this article was arranged by (*Corresponding author*: *Chee Hing Tan*).

George Basta, Jonathan Taylor-Mew, Im Sik Han, Mark Hopkinson, John P.R. David, Jo Shien Ng, and Chee Hing Tan are with the School of Electrical and Electronic Engineering, University of Sheffield, S1 3JD Sheffield, U.K. (e-mail: gbasta1@sheffield.ac.uk; j.taylor-mew@sheffield.ac.uk; i.han@sheffield.ac.uk; m.hopkinson@sheffield.ac.uk; j.p.david@sheffield.ac.uk; j.s.ng@sheffield.ac.uk; c.h.tan@sheffield.ac.uk).

Tarick Blain was with the School of Electrical and Electronic Engineering, The University of Sheffield, S1 3JD Sheffield, U.K. He is now with Phlux Technology, S1 4WP Sheffield, U.K. (e-mail: tarick.blain@phluxtechnology.com).

I. Introduction

HIGH performance avalanche photodiodes (APDs) are widely used in optical receivers for demanding optical applications, such as laser ranging [1], remote gas sensing [2] and Quantum Key Distribution [3]. Thanks to the internal avalanche gain, generated by a chain of impact ionization events, APDs provide a crucial improvement in the signal to noise ratio of optical receivers. However, the stochastic impact ionization process gives rise to an excess noise factor, F, that exacerbates the APD's shot noise such as the APD noise becomes

$$\sqrt{2qM^2\left(I_{ph}+I_d\right)F(M)B}\,, \tag{1}$$

where q is the electronic charge, M is the APD's gain, $F(M)$ is the gain-dependent excess noise factor, B is the system bandwidth, and I_{ph} and I_d are the unmultiplied photocurrent and dark current respectively. This equation is valid when both I_{ph} and I_d are injected from the same side of the high field avalanche region. For a given B and I_{ph}, minimizing $F(M)$ and I_d is critical to minimize the APD's noise. Minimizing $F(M)$ can be achieved by using avalanche materials with disparate electron and hole ionization coefficients, α and β, because $F(M) = kM + (1\text{-}k)(2\text{-}1/M)$, where $k = \beta/\alpha$ [4]. The more disparate the ionization coefficients, the smaller the k value and consequently F. In addition, avalanche materials with small k maximize the gain-bandwidth product of an APD [5]. Therefore, minimizing the k value has been actively pursued to achieve high performance APDs.

APDs for weak infrared signals primarily use a Separate Absorption Multiplication (SAM) structure, in which a narrow bandgap material absorbs the infrared optical signal, and a wider bandgap material generates the internal gain (without causing excessive band to band tunnelling current at high electric field). SAM APDs are most commonly found in telecommunications applications, and they exist in the form of InGaAs/InP SAM-APD, consisting of an InGaAs absorber and an InP avalanche region or multiplier. InP has $k \sim 0.3$ [6], which can be improved upon by an alternative avalanche material, $In_{0.52}Al_{0.48}As$ (k of 0.15 - 0.20 ([7,8]). However, both InP and $In_{0.52}Al_{0.48}As$ have relatively poor excess noise performance compared to Silicon APDs, but silicon has an optical absorption cut-off wavelength, λ_c, around 1000nm.

In recent years, two Sb-based alloys, AlGaAsSb and AlInAsSb, have emerged as promising avalanche materials due to their excellent low $F(M)$ characteristics. Initial works

focused on $AlAs_{0.56}Sb_{0.44}$, lattice-matched to InP substrates. These exhibited exceptionally low excess noise factor values, at $F \sim 2$ [9] with $k \sim 0.005$ [10]. $Al_{0.85}Ga_{0.15}As_{0.56}Sb_{0.44}$ (also lattice-matched to InP) also showed very low excess noise factor, with $F \sim 2$ at M up to 15 and 25 [11] [12]. Following the first InGaAs/$Al_{0.85}Ga_{0.15}As_{0.56}Sb_{0.44}$ SAM-APD demonstration in [13], subsequent SAM-APDs achieved low noise equivalent power (22 fW√Hz) [14] and room temperature single photon detection [15]. SAM-APDs using GaAsSb absorbers were also demonstrated to simplify the APD bandgap grading design [16] [17]. By combining an InGaAs/GaAsSb type II superlattice absorber with an $Al_{0.85}Ga_{0.15}As_{0.56}Sb_{0.44}$ avalanche region, results have shown that an extended optical absorption cut-off wavelength, λ_c, of up to 2.4 μm and an $F = 2$ at $M = 20$ can be achieved [18]. λ_c can be further extended by switching to AlGaAsSb and AlInAsSb alloys lattice matched to GaSb substrates (rather than InP substrates). A SAM-APD on GaSb substrate with an $In_{0.22}Ga_{0.78}As_{0.19}Sb_{0.81}$ absorber with an $Al_{0.9}Ga_{0.1}As_{0.08}Sb_{0.92}$ multiplier achieved $\lambda_c \sim 2.75$ μm but exhibited poor excess noise performance ($F = 4.5$ at $M = 20$) [19]. Better noise performance ($F = 2.2$ at $M = 10$) and longer λ_c (3.5 μm) were obtained using an $Al_{0.05}In_{0.95}AsSb$ absorber and an $Al_{0.7}In_{0.3}AsSb$ multiplier, both lattice-matched to GaSb substrate [20]. A wider bandgap avalanche material, $Al_{0.8}In_{0.2}AsSb$ (also lattice-matched to GaSb) exhibited $k \sim 0.05$ [21]. However, the SAM-APD quantum efficiency in this case was only ~ 5 % at 3.4 μm [20] and hence such an approach does not seem suitable for demanding optical applications above 3 μm, such as methane gas sensing at ~ 3.4 μm [22].

Electron-only APDs such as HgCdTe and InAs achieve the lowest excess noise factors in MWIR. HgCdTe (MCT) APDs can achieve F of 1.5 at gains > 189 with ~ 4.1 μm cut-off wavelength [23]; however, their deployment is often limited by the need for cryogenic cooling and by rigorous environmental and process controls in both material growth and fabrication. Bulk InAs is a good alternative but also requires some cooling. There is therefore interest in novel materials exhibiting very low $F(M)$ performance at room temperature for MWIR operation.

InAs is also an excellent candidate as an absorber material in MWIR SAM-APDs operating at room temperature. InAs photodiodes exhibit an external quantum efficiency over 50% at 3.35 μm [24] and could go further via the use of anti-reflection coatings. A SAM-APD on InAs substrate using an InAs absorber and an $AlAs_{0.15}Sb_{0.85}$ multiplier has been demonstrated [25] but had a relatively low intrinsic quantum efficiency (i.e. without avalanche gain) of 24 %, possibly due to an absence of bandgap grading between the narrow gap InAs and wide gap $AlAs_{0.15}Sb_{0.85}$.

There is a lack of excess noise reports for AlGaAsSb or AlInAsSb lattice-matched to InAs substrates. Such measurements would be important for developing high performance SAM-APD with $\lambda_c > 3$ μm. Therefore, in this work, we present a rigorous characterization of the excess noise characteristics of $Al_{0.8}In_{0.2}As_{0.31}Sb_{0.69}$ lattice-matched to InAs substrates, distinct from previous studies using GaSb substrates [21]. We have found that $Al_{0.8}In_{0.2}As_{0.31}Sb_{0.69}$ lattice-matched to InAs exhibits extremely low excess noise ($k \sim 0.02$ - 0.03) at high gain ($M > 100$). Our data serves as significant evidence that it is feasible to combine a low-noise wide bandgap multiplier with InAs absorber to achieve high performance APDs operating at room temperature for mid-wave infrared detection (up to 3.6 μm). The data reported in this manuscript is available from ORDA digital repository [26].

II. Experimental Details

A pair of homojunction $Al_{0.8}In_{0.2}As_{0.31}Sb_{0.69}$ (hereafter AlInAsSb) p-i-n and n-i-p diode wafers were grown on 2-inch (100) vertical gradient freeze n- or p-type doped InAs substrates by Molecular Beam Epitaxy using high quality group III evaporation sources and thermal cracker cells for the group V elements. This composition of $Al_{0.8}In_{0.2}As_{0.31}Sb_{0.69}$ is slightly different from that of [21] in terms of the group V ratio, because of a modest 0.6% difference in lattice constants between GaSb and InAs. The AlInAsSb layers were grown as a random alloy, and both wafers have a 100 nm n^+ InAs buffer layer on the n-type (or p-type) InAs substrate. This was followed by a nominally 1000 nm thick i- AlInAsSb layer sandwiched between a 200 nm p^+ AlInAsSb and a 500 nm n^+ AlInAsSb cladding layers. A top 50 nm p-type InAs contact layer was included for good ohmic contact. All the doped layers were intended to have a doping density of 1×10^{18} cm^{-3}. The n-i-p diode wafer was grown on a p-type substrate and has the same layer thicknesses as those of the p-i-n diode wafer.

We note that previous research on AlInAsSb avalanche properties (on GaSb substrates) have used AlInAsSb grown as digital alloy [20, 21]. However, experimental works on $Al_{0.85}Ga_{0.15}As_{0.56}Sb_{0.44}$ on InP substrates have used both digital alloy and random alloy growth, with negligible differences in the reported characteristics. In particular, a study comparing impact ionization coefficients of $Al_{0.85}Ga_{0.15}As_{0.56}Sb_{0.44}$ grown as digital alloy and random alloy has observed no difference [27]. Therefore, we do not anticipate the growth method used in our work to have significant effects on the excess noise characteristics of $Al_{0.8}In_{0.2}As_{0.31}Sb_{0.69}$ on InAs substrates.

The substrate temperature during wafer growth was maintained at 440 °C with a growth rate of ~ 1.2 Å/s. These were determined to be optimal following morphology and x-ray analysis of a range of conditions in this material system that is prone to miscibility effects and thermal roughening. The quaternary samples are grown under a slight Sb_2 excess flux from an un-valved antimony cracker, with the lattice match controlled by a valved arsenic cracker providing a precise As_2 flux. We used the conventional III-V dopants of Si and Be. Whilst these appear to be effective dopants in this material system, questions remain over their complete activation. Detailed growth and dopant investigations will be the subject of further reports. The exact same growth conditions were used for p-i-n and n-i-p diodes.

Experimental photoluminescence measurements obtained from a small unprocessed piece of the wafer indicate a peak wavelength of ~ 882 nm at room temperature. This corresponds to a bandgap of 1.41 eV for the AlInAsSb alloy used in this work.

Mesa APDs with diameters of 400 and 200 μm were fabricated from pieces of the p-i-n wafer using standard contact

photolithography and wet-etching solutions. The fabricated p-i-n diode is shown schematically in Fig. 1. The top and back metal contacts were 20/200 nm Ti/Au deposited via sputtering. Prior to the top contact deposition, native oxide was removed by a plasma asher. Mesa structures were created using a wet-etching solution composed of citric acid (40 g), H_3PO_4 (10 ml), H_2O_2 (10 ml), and deionized water (240 ml) [28]. Slightly larger mesa diodes with diameters of 420 and 220 µm were also fabricated from the n-i-p wafer. No surface passivation or anti-reflection coatings were applied.

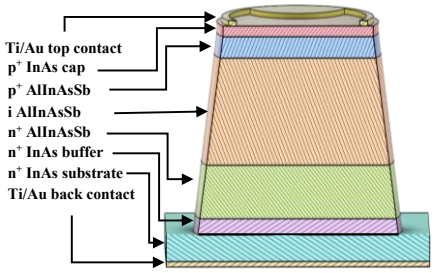

Fig. 1. Schematic diagram of the AlInAsSb p-i-n diode (not drawn to scale).

The large diodes (400 and 420 µm) and the small diodes (200 and 220 µm) were characterized using current-voltage (I-V), capacitance-voltage (C-V), photoresponse, avalanche gain and excess noise measurements. Data were obtained from a minimum of three devices for each type of measurement. The I-V characteristics were measured using a picoammeter. The ideality factor was extracted from the forward I-V data, while the leakage current and breakdown voltage were obtained from the reverse I-V data. The C-V characteristics were obtained using an LCR meter. The built-in voltage was estimated by extrapolating $1/C(V)^2$ to zero, yielding a value of 1.07 V.

Prior to the C-V fittings, we investigated experimentally the background doping type of the i-AlInAsSb layers. Using the same two wafers, additional partially etched p-i-n and n-i-p AlInAsSb devices (down to approximately half of the i-region thickness) were produced. At a reverse bias of 10 V, the measured capacitance was 30 pF for partially etched p-i-n diodes, compared to 20 pF for fully etched p-i-n diodes. The higher capacitance of the partially etched p-i-n diode indicates that the depletion region is not entirely confined within the partially etched mesa. Conversely, the capacitance values were identical for both partially and fully etched n-i-p diodes, indicating complete depletion confinement within the mesa structure. This technique was used to identify the unintended background doping type in mesa diodes [29]. These results indicate that the unintended background doping in the i-AlInAsSb layers is p-type.

Using a 1-D Poisson Electric-field solver, fittings were conducted on the experimental C-V characteristics to estimate the layer thicknesses and doping concentrations. A relative dielectric constant of 11.88 obtained from linear interpolation of the constituent binary alloys (AlAs, AlSb, InAs, and InSb) [30] was used for AlInAsSb. For clarity of the presentation, the experimental C-V data and fittings are shown for only the large p-i-n and n-i-p diodes in Fig. 2. The large and small devices' capacitance scaled with area (not shown here). The C-V fittings use the nominal values for layer thickness, but doping concentrations used for the doped AlInAsSb cladding layers are between 1×10^{17} cm^{-3} and 3×10^{17} cm^{-3}, which are lower than the nominal values. Also, the C-V fittings suggest unintentional background doping of 1×10^{16} cm^{-3} and 2×10^{16} cm^{-3} in the p-i-n and n-i-p diodes, respectively. The estimated electric field profiles at a reverse bias of 50 V indicate that, for a given reverse bias, the n-i-p diode has a higher peak electric field than the p-i-n diode (537 compared to 492 kV/cm). The extracted electric field profiles were used to (i) inform whether there is a significant change in depletion width in the p^+ and n^+ layers as reverse bias increases and (ii) predict the dependence of photocurrent (or the primary current) on reverse bias. The primary current was subsequently used to obtain the gain (or multiplication factor), given by the ratio of total photocurrent to the primary photocurrent.

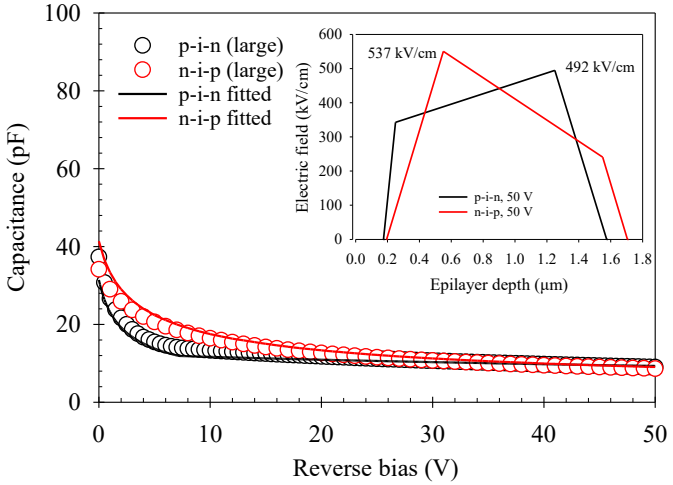

Fig. 2. Experimental capacitance-voltage characteristics (symbols) and fittings (lines) of large p-i-n and n-i-p diodes, with estimated electric field profiles at a reverse bias of 50 V in the inset.

Avalanche gain, shot noise, and excess noise measurements were conducted using a setup described in [31]. Optical signals at wavelengths of 543, 625 and 850 nm were modulated and focused onto the optical window of the device-under-test. The setup utilized a phase-sensitive detection technique for measuring the photocurrent and noise power, following amplification by a transimpedance amplifier (TIA), with lock-in amplifiers. This distinguishes the signals from dark current, background interference and electronic noise, facilitating accurate $F(M)$ measurements. The optical power remaining inside the diode for each wavelength was estimated using $I = I_0(1-R)e^{-\gamma \cdot W}$, where I_0 is the incident optical power, R is the reflectivity of the semiconductor surface, γ is the absorption coefficient for a given wavelength, and W is the width of the absorption region. Values of γ in AlInAsSb were estimated from linear interpolation of the constituent binary alloys [30], which yielded 9.8×10^4, 6.3×10^4 and 1.1×10^4 cm^{-1} for 543, 625 and 850 nm, respectively. The 543 nm wavelength light is fully absorbed (> 99 %) by the top two layers, p^+ (or n^+) InAs cap and p^+ (or n^+) AlInAsSb cladding layer, giving rise to a pure electron (or hole) injection profile in the p-i-n (or n-i-p) diodes. At longer wavelengths of 625 and 850 nm, the proportion of light absorbed by the top two layers decreases to ~94 and 45 %, respectively. These longer wavelengths, therefore, produce mixed carrier injection profiles.

III. Results

Room temperature dark I-V characteristics for both p-i-n and n-i-p diodes are shown in Fig. 3. Under forward bias, the diodes exhibited an ideality factor of 1.8. The n-i-p diodes showed higher series resistance in the forward I-V than the p-i-n diodes. This is attributed to the relatively low doping concentration of the top n^+ AlInAsSb cladding layer (1×10^{17} cm^{-3}). In the reverse bias, the breakdown voltage (defined as the voltage corresponding to a dark current of 100 μA) is 58.5 and 52.3 V for the p-i-n and n-i-p diodes, respectively. The smaller breakdown voltage in the n-i-p diode is attributed to the higher peak electric field (caused by its higher unintended background doping in its i-AlInAsSb layer) shown in Fig. 2. In the p-i-n diode, the dark current increases proportionally with diode area, as expected when the dark currents are dominated by bulk leakage mechanism(s). The measured dark currents do not appear to be dominated by tunnelling currents over the voltage ranged used. In contrast, the different-sized n-i-p diodes exhibit similar dark currents, indicating significant surface leakage currents. Nevertheless, the dark I-V characteristics of the p-i-n and n-i-p diodes confirm that the devices are sufficiently robust for subsequent measurements.

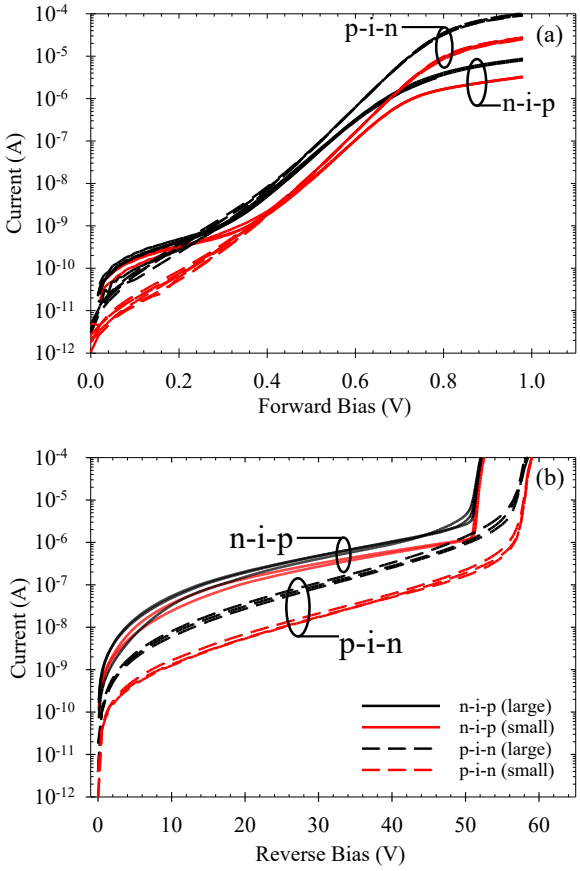

Fig. 3. (a) Forward and reverse (b) bias current-voltage characteristics for p-i-n and n-i-p diodes.

Avalanche gain data for 543, 625 and 850 nm optical signals of the p-i-n diodes are shown in Fig. 4(a), together with the lock-in amplifier signal shown in the inset. Data from large and small diodes are in agreement, although only results from the large diodes are presented here for clarity. For a given reverse bias, as the optical signal wavelength decreases, gain increases. Since decreasing wavelength increases the proportion of electrons in the carrier injection profile, we can conclude from the gain data that pure electron injection produces higher gain than mixed carrier injection. This indicates $\alpha>\beta$. In the inset of Fig. 4, the lock-in amplifier signal increases rapidly at low reverse bias (0 to 7.5 V). These are most pronounced in data obtained using the shortest wavelength (543 nm), which is expected from its greater dependence on the photo-generated carrier collection efficiency with reverse bias.

The experimental $F(M)$ results of the p-i-n diodes for different carrier injection profiles are compared in Fig. 4(b). For a given M, F is the lowest under pure electron injection (543 nm wavelength) and increases rapidly as more mixed injection occurs (longer wavelengths). This is consistent with the observation, $\alpha > \beta$ drawn from Fig. 4(a). For rigor, additional $F(M)$ measurements using optical signals at 543 nm were performed on 12 p-i-n and 8 n-i-p diodes for pure electron and pure hole injection, respectively. The data are shown in Fig. 5(a), confirming very low $F(M)$ from the p-i-n diode (with pure electron injection) that correspond to $0 < k < 0.04$ [4] and very high $F(M)$ from the n-i-p diode (with pure hole injection).

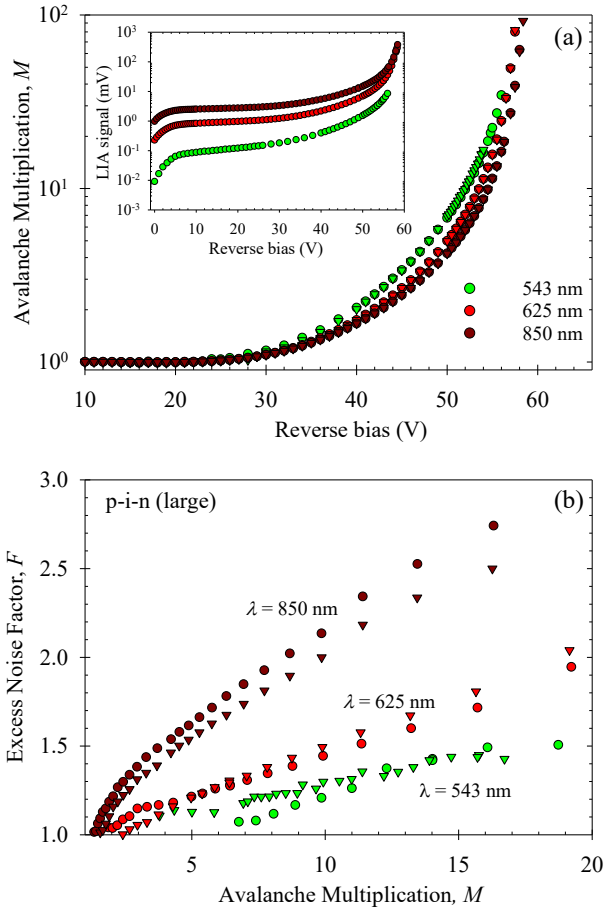

Fig. 4. (a) Experimental avalanche gain of the large p-i-n diodes obtained using optical signals at 543, 625, and 850 nm wavelengths. The inset shows the corresponding photocurrent signals from the Lock-in Amplifier (LIA). (b) Corresponding experimental excess noise factor versus avalanche gain for the three wavelengths.

Slightly higher $F(M)$ data from small-sized p-i-n diodes compared to the large p-i-n diodes can be observed in Fig. 5(a). We attribute this discrepancy to unintended mixed injection, which is possibly due to reflected stray light entering the diodes through their mesa sidewalls, an observation based on a further set of $F(M)$ data. These were obtained from additional devices fabricated with a metal optical mask covering the mesa sidewalls to prevent unintentional side injection, giving rise to mixed injection. The $F(M)$ data from these p-i-n diodes with optical masks clearly correspond to $0 < k < 0.03$, as shown in Fig. 5(b). At $M = 100$, $F \sim 3.9$-4.9 corresponding to $k = 0.02$-0.03. In contrast, under pure hole injection, the n-i-p diodes exhibited very high excess noise, $F > 17$ at $M \sim 3$. Therefore, our comprehensive $F(M)$ data (from 15 p-i-n diodes and 12 n-i-p diodes) show that $\alpha >> \beta$ in this alloy.

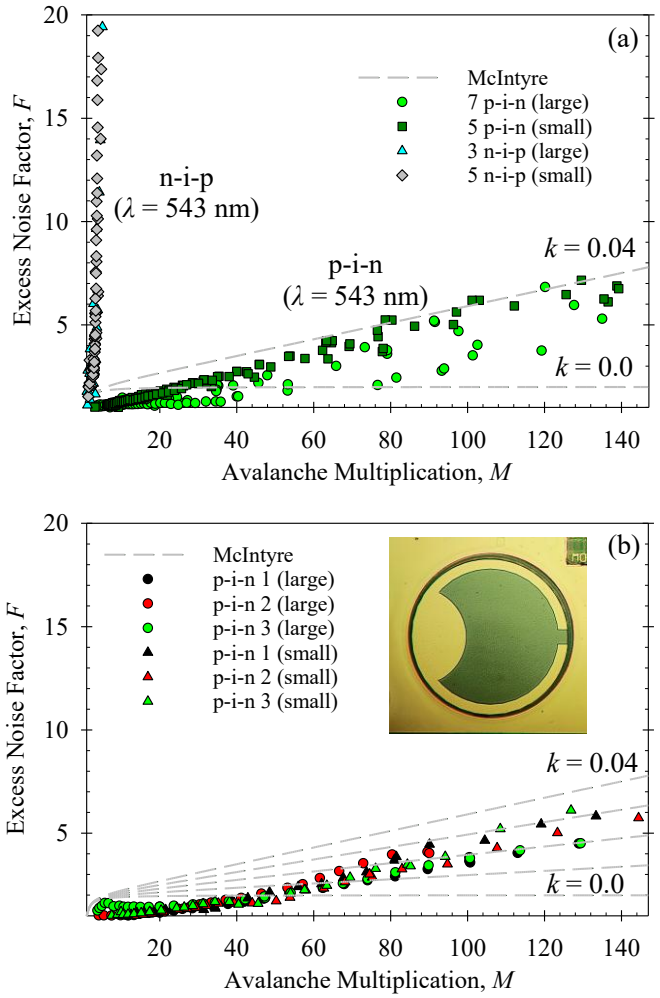

Fig. 5. (a) $F(M)$ data using 543 nm wavelength from different-sized p-i-n and n-i-p diodes without optical masks. (b) Different-sized p-i-n diodes with optical mask. The lines which come from the McIntyre model increase from $k = 0$ to 0.04 in steps of 0.01. Inset shows a large mesa with the optical mask.

IV. Discussion

Given the very low excess noise in Fig. 4 and Fig. 5, it is essential to check that there is no unintended attenuation of the noise signal during the $F(M)$ measurements. First, we compared the shot noise versus photocurrent characteristics obtained from the three large AlInAsSb p-i-n diodes of this work (reverse biased at 20 and 25 V, hence unity avalanche gain) with those from a reference commercial Si photodiode (BPX-65; reverse biased at 5 V). In these measurements, the optical signal from a 633 nm He-Ne laser was attenuated using a variable optical filter. The shot noise data are shown in Fig. 6. The data from the three large AlInAsSb p-i-n diodes and the Si photodiode are in agreement and exhibit the expected linear dependence of noise signal on photocurrent. Hence, the AlInAsSb p-i-n diodes, prior to appreciable avalanche gain, do exhibit typical shot noise.

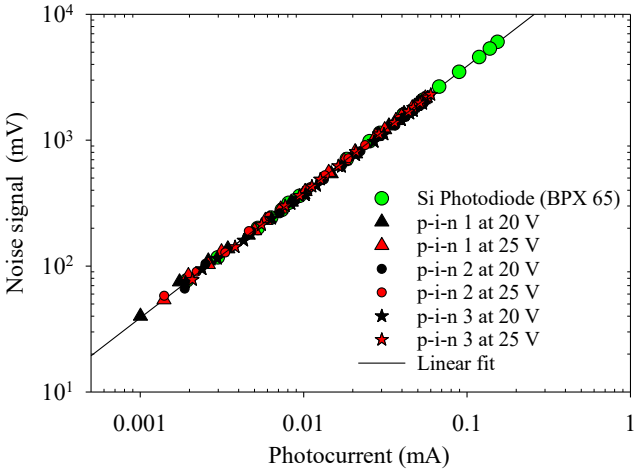

Fig. 6. Measured shot noise from a reference Si photodiode and three large AlInAsSb p-i-n diodes.

Next, we measured the noise power spectra of the AlInAsSb p-i-n diodes using a Rigol DSA832 spectrum analyzer to check if there was unintended distortion of the noise spectra. The experimental noise spectra at reverse bias of 20 to 56 V are compared in Fig. 7. Between 20 and 40 V, noise from avalanche gain is very small (due to low gain), so the overall noise from the setup is dominated by the amplifier noise. The noise power spectra at 50 V and above exceeded the amplifier noise floor and remained flat up to ~ 10 MHz before rolling off. These are typical features of noise power spectra obtained from our setup when using diodes/APDs made with other materials, confirming the accuracy of our $F(M)$ data shown in Fig. 4 and Fig. 5.

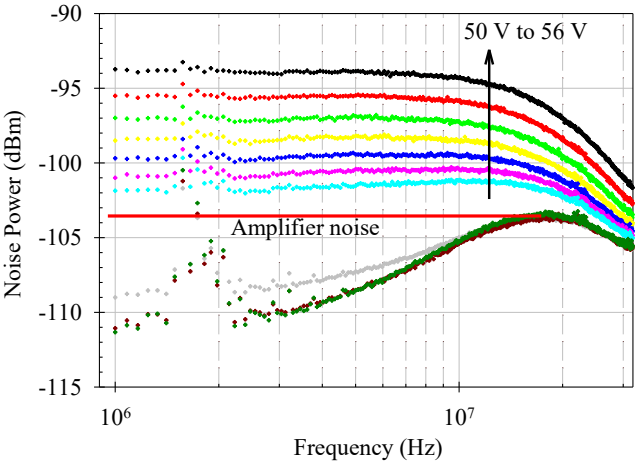

Fig. 7. Measured noise power at different voltages for the p-i-n wafer when illuminated with a 633 nm laser. Data below the amplifier noise were measured at 20, 30, and 40 V, while data above the amplifier noise were measured at 50 to 56 V in 1 V steps.

The very low $F(M)$ characteristics obtained from the $Al_{0.8}In_{0.2}AsSb$ p-i-n diode lattice-matched to InAs substrate of this work are similar to reports using other Sb-containing alloys. They include $Al_{0.85}Ga_{0.15}AsSb$ lattice matched to InP [11,12] and AlInAsSb lattice matched to GaSb [32]. Therefore, AlInAsSb can be a low-noise multiplier with an InAs absorber in a SAM-APD for high-efficiency detection of wavelengths above that of InGaAs-based SAM-APDs.

To achieve a SAM-APD with high quantum efficiency at wavelengths > 3000 nm, InAs is an excellent candidate material for the absorption region, as it has higher quantum efficiency at wavelengths > 1550 nm compared to other materials, as mentioned in Section I. The external quantum efficiency of InAs [24] is compared with those reported from $Al_{0.15}InAsSb$ [33], $Al_{0.05}InAsSb$ [20], $In_{0.22}Ga_{0.78}As_{0.19}Sb_{0.81}$ [19], and Type II InGaAs/GaAsSb grown on InP [18] in

Fig. *8*. Clearly, InAs is superior at wavelengths > 3000 nm. A proof-of-concept SAM-APD using an InAs absorption region has been reported by [25]. They demonstrated that with avalanche gain, a responsivity as high as 8 A/W at a wavelength of 3.27 μm could be achieved. A comparison of relevant avalanche materials for MWIR detection (e.g. InAs and HgCdTe) as well as other AlInAsSb reports is presented in Table. 1. At avalanche gain of ~15, the excess noise factor of this work is comparable to values exhibited by InAs and HgCdTe, but slightly lower than previous reports of AlInAsSb (on GaSb or InP substrates). Relative to HgCdTe, the $Al_{0.8}In_{0.2}AsSb$ avalanche layer is much wider bandgap. Hence, an InAs/$Al_{0.8}In_{0.2}AsSb$ MWIR SAM-APD can operate high gain without limitation of band-to-band tunnelling current. However, the challenge, to carefully optimize the bandgap grading to achieve smooth electron transport from InAs to $Al_{0.8}In_{0.2}AsSb$, will need to be solved.

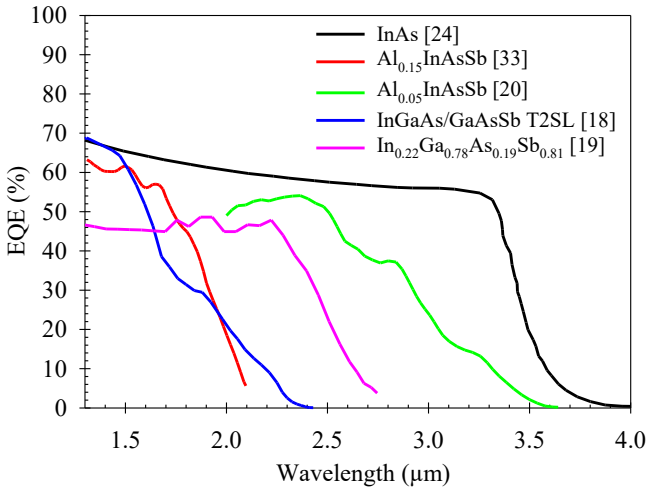

Fig. 8. Comparison of reported external quantum efficiency (EQE) of different absorbers.

Table 1. Comparison of relevant avalanche materials for MWIR and other AlInAsSb reports

Ref	Avalanche Material (substrate)	Operating Temperature (K)	Excess Noise Factor ($M \sim 15$)
This work	**$Al_{0.8}In_{0.2}As_{0.31}Sb_{0.69}$ (InAs)**	**300**	**~ 1.1**
[20]	$Al_{0.7}InAsSb$ (GaSb)	100	~ 2.6
[21]	$Al_{0.8}InAsSb$ (GaSb)	300	~ 3.1
[35]	$Al_{0.7}InAsSb$ (InP)	300	~ 2.0
[34]	InAs (InAs)	250	~ 1.5
[23]	HgCdTe (CdZnTe)	80	~ 1.5

V. Conclusion

Random alloy $Al_{0.8}In_{0.2}As_{0.31}Sb_{0.69}$ p-i-n and n-i-p diodes were grown using molecular beam epitaxy and characterized at room temperature. Both p-i-n and n-i-p diodes show well-defined avalanche breakdown in the reverse bias, with an avalanche gain above 100 in the p-i-n diodes. Comparisons of gain characteristics from different carrier injection profiles clearly indicate that $\alpha > \beta$. Rigorous excess noise measurements of p-i-n and n-i-p diodes confirm that $\alpha >> \beta$, with excess noise factors of the p-i-n diodes being the lowest (best) under pure electron injection ($F \sim 3.9$-4.9 at $M = 100$) and increasing rapidly with mixed carrier injection. Also, the excess noise factors obtained under pure hole injection from n-i-p diodes are very high ($F > 17$ at $M \sim 3$). Additional experimental measurements (noise power versus photocurrent and noise power versus frequency) confirmed that our excess noise measurements data are robust. Therefore, $Al_{0.8}In_{0.2}As_{0.31}Sb_{0.69}$ lattice-matched to InAs substrates is a very low noise avalanche material that can be combined with an InAs absorber. The combination can potentially provide APDs with excellent quantum efficiency at wavelengths above 3 μm, which is of particular importance for methane gas sensing at ~ 3.4 μm.

References

[1] S. K. Poultney, 'Single Photon Detection and Timing in the Lunar Laser Ranging Experiment', *IEEE Trans. Nucl. Sci.*, vol. 19, no. 3, pp. 12–17, 1972, doi: 10.1109/TNS.1972.4326697.

[2] J. Titchener, D. Millington-Smith, C. Goldsack, G. Harrison, A. Dunning, X. Ai, and M. Reed, 'Single photon Lidar gas imagers for practical and widespread continuous methane monitoring', *Appl. Energy*, vol. 306, p. 118086, Jan. 2022, doi: 10.1016/j.apenergy.2021.118086.

[3] N. Gisin, G. Ribordy, W. Tittel, and H. Zbinden, 'Quantum cryptography', *Rev. Mod. Phys.*, vol. 74, no. 1, pp. 145–195, Mar. 2002, doi: 10.1103/RevModPhys.74.145.

[4] R. J. McIntyre, 'Multiplication noise in uniform avalanche diodes', *IEEE Trans. Electron Devices*, vol. ED-13, no. 1, pp. 164–168, Jan. 1966, doi: 10.1109/T-ED.1966.15651.

[5] R. B. Emmons, 'Avalanche-Photodiode Frequency Response', *J. Appl. Phys.*, vol. 38, no. 9, pp. 3705–3714, Aug. 1967, doi: 10.1063/1.1710199.

[6] L. J. J. Tan, J. S. Ng, C. H. Tan, and J. P. R. David, 'Avalanche Noise Characteristics in Submicron InP

Diodes', *IEEE J. Quantum Electron.*, vol. 44, no. 4, pp. 378–382, Apr. 2008, doi: 10.1109/JQE.2007.914771.

[7] Shiyu Xie, Shiyong Zhang, and Chee Hing Tan, 'InGaAs/InAlAs Avalanche Photodiode With Low Dark Current for High-Speed Operation', *IEEE Photonics Technol. Lett.*, vol. 27, no. 16, pp. 1745–1748, Aug. 2015, doi: 10.1109/LPT.2015.2439153.

[8] W. Wang, J. Yao, L. Li, H. Ge, L. Wang, L. Zhu, Q. Chen, H. Lu, and B. Chen, 'High-speed InAlAs digital alloy avalanche photodiode', *Appl. Phys. Lett.*, vol. 123, no. 19, p. 191102, Nov. 2023, doi: 10.1063/5.0169935.

[9] X. Yi, S. Xie, B. Liang, L. W. Lim, J. S. Cheong, M. C. Debnath, D. L. Huffaker, C. H. Tan, and J. P. R. David, 'Extremely low excess noise and high sensitivity AlAs0.56Sb0.44 avalanche photodiodes', *Nat. Photonics*, vol. 13, no. 10, pp. 683–686, Oct. 2019, doi: 10.1038/s41566-019-0477-4.

[10] X. Yi, S. Xie, B. Liang, L. W. Lim, X. Zhou, M. C. Debnath, D. L. Huffaker, C. H. Tan, and John. P. R. David, 'Demonstration of large ionization coefficient ratio in AlAs0.56Sb0.44 lattice matched to InP', *Sci. Rep.*, vol. 8, no. 1, p. 9107, Jun. 2018, doi: 10.1038/s41598-018-27507-w.

[11] S. Lee, S. H. Kodati, B. Guo, A. H. Jones, M. Schwartz, M. Winslow, C. H. Grein, T. J. Ronningen, J. C. Campbell, and S. Krishna, 'Low noise Al0.85Ga0.15As0.56Sb0.44 avalanche photodiodes on InP substrates', *Appl. Phys. Lett.*, vol. 118, no. 8, p. 081106, Feb. 2021, doi: 10.1063/5.0035571.

[12] J. Taylor-Mew, V. Shulyak, B. White, C. H. Tan, and J. S. Ng, 'Low Excess Noise of $Al_{0.85}$ $Ga_{0.15}$ $As_{0.56}$ $Sb_{0.44}$ Avalanche Photodiode From Pure Electron Injection', *IEEE Photonics Technol. Lett.*, vol. 33, no. 20, pp. 1155–1158, Oct. 2021, doi: 10.1109/LPT.2021.3110123.

[13] S. Xie, X. Zhou, S. Zhang, D. J. Thomson, X. Chen, G. T. Reed, J. S. Ng, and C. H. Tan, 'InGaAs/AlGaAsSb avalanche photodiode with high gain-bandwidth product', *Opt. Express*, vol. 24, no. 21, p. 24242, Oct. 2016, doi: 10.1364/OE.24.024242.

[14] B. Sheridan, X. Collins, J. Taylor-Mew, B. White, J. S. Ng, and C. H. Tan, 'An Extremely Low Noise-Equivalent Power Photoreceiver Using High-Gain InGaAs/AlGaAsSb APDs', *J. Light. Technol.*, vol. 43, no. 2, pp. 741–746, Jan. 2025, doi: 10.1109/JLT.2024.3447284.

[15] J. Taylor-Mew, L. Li, T. Blain, C. H. Tan, and J. S. Ng, 'Room Temperature InGaAs/AlGaAsSb Single Photon Avalanche Diode', *IEEE Photonics J.*, vol. 17, no. 2, pp. 1–6, Apr. 2025, doi: 10.1109/JPHOT.2025.3541323.

[16] Y. Cao, T. Blain, J. D. Taylor-Mew, L. Li, J. S. Ng, and C. H. Tan, 'Extremely low excess noise avalanche photodiode with GaAsSb absorption region and AlGaAsSb avalanche region', *Appl. Phys. Lett.*, vol. 122, no. 5, p. 051103, Jan. 2023, doi: 10.1063/5.0139495.

[17] S. Lee, X. Jin, H. Jung, H. Lewis, Y. Liu, B. Guo, S. H. Kodati, M. Schwartz, C. Grein, T. J. Ronningen, J. P. R. David, Joe. C. Campbell, and S. Krishna, 'High gain, low noise 1550 nm GaAsSb/AlGaAsSb avalanche photodiodes', *Optica*, vol. 10, no. 2, p. 147, Feb. 2023, doi: 10.1364/OPTICA.476963.

[18] H. Jung, S. Lee, X. Jin, Y. Liu, Theodore. J. Ronningen, Christopher. H. Grein, John. P. R. David, and S. Krishna, 'Low excess noise and high quantum efficiency avalanche photodiodes for beyond 2 μm wavelength detection', *Commun. Mater.*, vol. 5, no. 1, p. 219, Oct. 2024, doi: 10.1038/s43246-024-00627-9.

[19] X. Jin, S. Zhao, A. P. Craig, Q. Tian, L. Gilder, X. Yi, M. Carmichael, T. Golding, C. H. Tan, A. R. J. Marshall, and J. P. R. David, 'High-performance room temperature 2.75 μm cutoff $In_{0.22}$ $Ga_{0.78}$ $As_{0.19}$ $Sb_{0.81}$ /$Al_{0.9}$ $Ga_{0.1}$ $As_{0.08}$ $Sb_{0.92}$ avalanche photodiode', *Optica*, vol. 11, no. 12, p. 1632, Dec. 2024, doi: 10.1364/OPTICA.539859.

[20] A. A. Dadey, J. A. McArthur, A. Kamboj, S. R. Bank, D. Wasserman, and J. C. Campbell, 'High-gain low-excess-noise MWIR detection with a 3.5- μ m cutoff AlInAsSb-based separate absorption, charge, and multiplication avalanche photodiode', *APL Photonics*, vol. 8, no. 3, p. 036101, Mar. 2023, doi: 10.1063/5.0136918.

[21] A.-K. Rockwell, Y. Yuan, A. H. Jones, S. D. March, S. R. Bank, and J. C. Campbell, '$Al_{0.8}$ $In_{0.2}$ $As_{0.23}$ $Sb_{0.77}$ Avalanche Photodiodes', *IEEE Photonics Technol. Lett.*, vol. 30, no. 11, pp. 1048–1051, Jun. 2018, doi: 10.1109/LPT.2018.2826999.

[22] F. Song, C. Zheng, W. Yan, W. L. Ye, Y. Zhang, Y. Wang, and F. K. Tittel, 'Performance Enhancement of Methane Detection Using a Novel Self-Adaptive Mid-Infrared Absorption Spectroscopy Technique', *IEEE Photonics J.*, vol. 10, no. 6, pp. 1–12, Dec. 2018, doi: 10.1109/JPHOT.2018.2882391.

[23] L. Zhu, Z. Wang, J. Lin, J. Huang, L. He, X. Wang, S. Zhou, Z. Gan, X. Li, Q. Li, L. He, C. Lin, C. Lin, and B. Chen, 'High-temperature mid-wavelength infrared avalanche photodiode with modified fully-depleted absorption and multiplication region', Commun Mater, vol. 6, no. 1, p. 71, Apr. 2025, doi: 10.1038/s43246-025-00787-2.

[24] X. Zhou, X. Meng, A. B. Krysa, J. R. Willmott, J. S. Ng, and C. H. Tan, 'InAs Photodiodes for 3.43 μm Radiation Thermometry', *IEEE Sens. J.*, vol. 15, no. 10, pp. 5555–5560, Oct. 2015, doi: 10.1109/JSEN.2015.2443563.

[25] J. Huang, C. Zhao, B. Nie, S. Xie, D. C. M. Kwan, X. Meng, Y. Zhang, D. L. Huffaker, and W. Ma, 'High-performance mid-wavelength InAs avalanche photodiode using $AlAs_{0.13}$ $Sb_{0.87}$ as the multiplication layer', *Photonics Res.*, vol. 8, no. 5, p. 755, May 2020, doi: 10.1364/PRJ.385177.

[26] G. Basta, T. Blain, J. Taylor-Mew, I. S. Han, M. Hopkinson, J. P. R. David, J. S. Ng, and C. H. Tan, 'Dataset: Low Excess Noise $Al_{0.8}In_{0.2}As_{0.31}Sb_{0.69}$ Avalanche Photodiodes Lattice Matched to InAs'. doi: 10.15131/shef.data.29402042.

[27] B. Guo, X. Jin, S. Lee, S. Z. Ahmed, A. H. Jones, X. Xue, B. Liang, H. I. J. Lewis, S. H. Kodati, D. Chen, T. J. Ronningen, C. H. Grein, A. W. Ghosh, S. Krishna, J. P. R. David, and J. C. Campbell, 'Impact Ionization Coefficients of Digital Alloy and Random Alloy Al 0.85 Ga 0.15 As 0.56 Sb 0.44 in a Wide Electric Field Range', J. Lightwave Technol., vol. 40, no. 14, pp. 4758–4764, Jul. 2022, doi: 10.1109/JLT.2022.3169008.

[28] S. H. Kodati, S. Lee, B. Guo, A. H. Jones, M. Schwartz, M. Winslow, N. A. Pfiester, C. H. Grein, T. J. Ronningen, J. C. Campbell, and S. Krishna, 'AlInAsSb avalanche photodiodes on InP substrates', *Appl. Phys. Lett.*, vol. 118, no. 9, p. 091101, Mar. 2021, doi: 10.1063/5.0039399.

[29] P. J. Ker, 'Development of high speed low noise InAs electron avalanche photodiodes', University of Sheffield, 2012.

[30] S. Adachi, *Properties of Group-IV, III-V and II-VI Semiconductors*, 1st ed. Wiley, 2005. doi: 10.1002/0470090340.

[31] K. F. Li, D. S. Ong, J. P. R. David, R. C. Tozer, G. J. Rees, S. A. Plimmer, K. Y. Chang, and J. S. Roberts, 'Avalanche noise characteristics of thin GaAs structures with distributed carrier generation [APDs]', *IEEE Trans. Electron Devices*, vol. 47, no. 5, pp. 910–914, May 2000, doi: 10.1109/16.841220.

[32] S. R. Bank, J. C. Campbell, S. J. Maddox, M. Ren, A. K. Rockwell, M. E. Woodson, and S. D. March, 'Avalanche Photodiodes Based on the AlInAsSb Materials System', *IEEE J. Sel. Top. Quantum Electron.*, vol. 24, no. 2, pp. 1–7, Mar. 2018, doi: 10.1109/JSTQE.2017.2737880.

[33] A. H. Jones, S. D. March, S. R. Bank, and J. C. Campbell, 'Low-noise high-temperature AlInAsSb/GaSb avalanche photodiodes for 2-μm applications', *Nat. Photonics*, vol. 14, no. 9, pp. 559–563, Sep. 2020, doi: 10.1038/s41566-020-0637-6.

[34] P. J. Ker, J. P. R. David, and C. H. Tan, 'Temperature dependence of gain and excess noise in InAs electron avalanche photodiodes', Opt. Express, vol. 20, no. 28, p. 29568, Dec. 2012, doi: 10.1364/OE.20.029568.

[35] T. J. Ronningen, S. H. Kodati, X. Jin, S. Lee, H. Jung, X. Tao, H. I. J. Lewis, M. Schwartz, N. Gajowski, P. Martyniuk, B. Guo, A. H. Jones, J. C. Campbell, C. Grein, J. P. R. David, and S. Krishna, 'Ionization coefficients and excess noise characteristics of AlInAsSb on an InP substrate', Applied Physics Letters, vol. 123, no. 13, p. 131110, Sep. 2023, doi: 10.1063/5.0165800.